

Supporting Information

Supramolecular Isomerism of Coordination Compounds Based on the in Situ Formed $[V_2O_3]^{4+}$ Core: Discrete and Chain-like Architectures

Mirta Rubčić^{a*}, Ivan Halasz^b, Gordana Pavlović^c, Damir Pajić^d, Edi Topić^a, and Marina Cindrić^a

^a*Department of Chemistry, Faculty of Science, University of Zagreb, Horvatovac 102a, Zagreb 10000, Croatia*

^b*Ruđer Bošković Institute, Bijenička cesta 54, 10000 Zagreb, Croatia*

^c*Faculty of Textile Technology, University of Zagreb, Prilaz baruna Filipovića 28a, 10000 Zagreb, Croatia*

^d*Department of Chemistry, Faculty of Science, University of Zagreb, Horvatovac 102a, Zagreb 10000, Croatia*

1. Details of powder diffraction analysis.....	2
Figure S2.....	4
2. Magnetic measurements.....	5
3. Molecular and crystal structures.....	6
4. IR spectroscopy.....	22
5. Thermal analysis.....	25
6. References.....	28

1. Details of powder diffraction analysis

Bruker D8 Advance powder diffractometer, $\text{CuK}\alpha_1$ radiation from a primary Ge(111)-Johannson monochromator, Våntag-1 position sensitive detector with 6° angle opening; step mode with 0.0085° per step; the sample was contained in a 0.5 mm radius borosilicate glass capillary which was spun during data collection to improve particle statistics. High-resolution pattern of **1** was collected in the angle region from 4° to 70° in 2θ and the total data collection time was 16 h. Powder pattern was indexed using an orthorhombic unit cell which was found by Topas. Correct unit cell parameters as well as peak shape parameters were determined in a Le Bail type fit. Crystal structure was solved by parallel tempering global optimization assuming the molecular structure given in Scheme 1 using the program Fox.¹ Molecular structure was taken from the crystal structure of **1**. Global optimization restrained bond lengths and angles to their expected values, leaving torsion angles free to allow for the correct conformation to be found. Among the optimized structure models, the most likely one was selected based on chemical reasoning (reasonable conformation, no too close contacts). Additionally, chemical meaningfulness could be estimated by formation of V=O...V close contact. The best obtained model was introduced into Rietveld refinement which was accomplished using the program Topas.² The structure was refined with restraints on bond lengths and angles as well as planarity restraints.

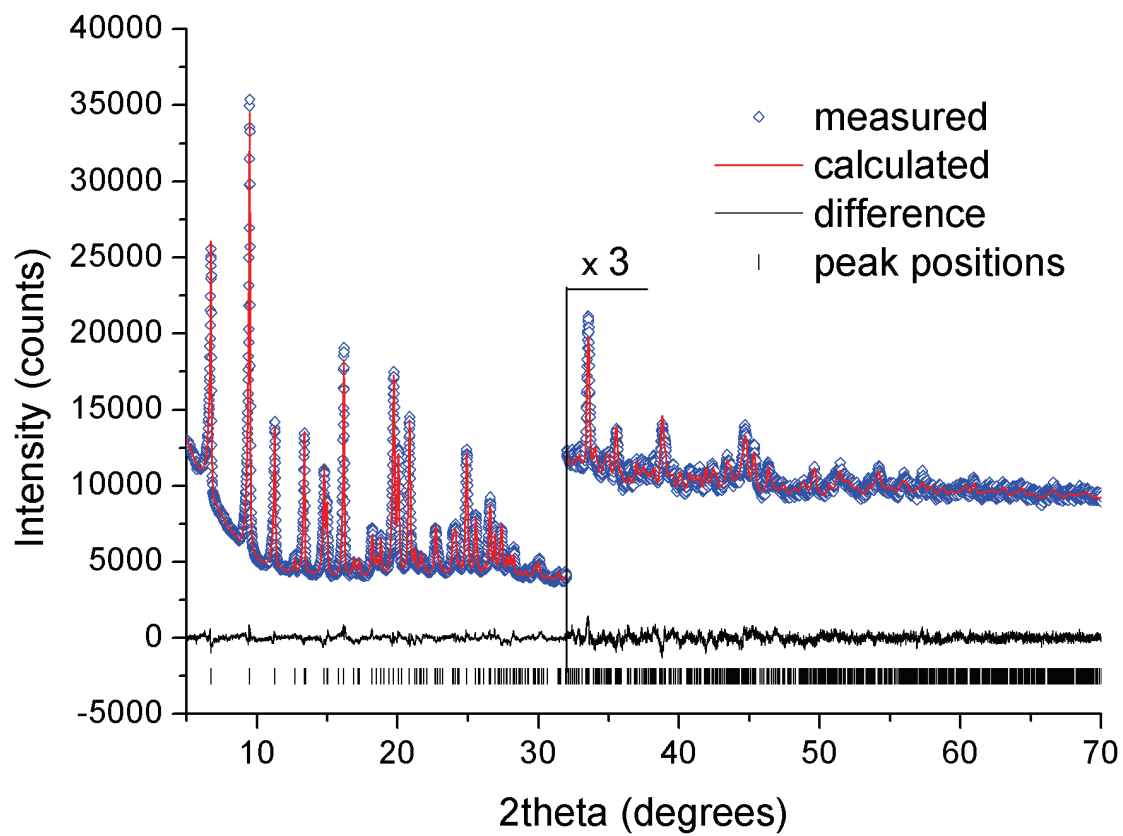


Figure S1. Rietveld plot for **1**. The high angle region starting from 32° is multiplied by a factor of 3 for clarity.

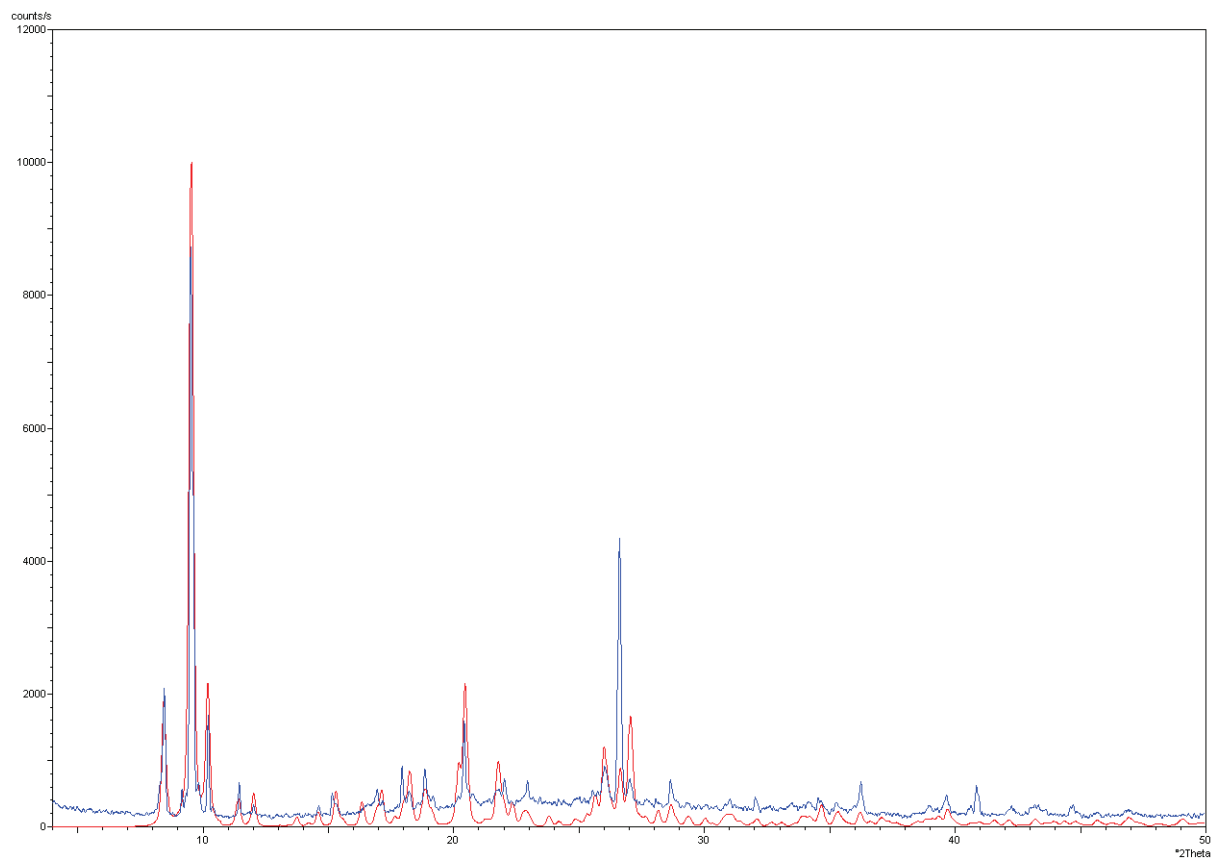


Figure S2. Comparison of simulated diffraction pattern for $[\text{V}_2\text{O}_3(\text{HL})(\text{OCH}_3)]_2 \cdot 4\text{CH}_3\text{OH}$ (3) (red) and the experimental one collected after exposing sample (not grinded) to air for 1 hour (blue).

2. Magnetic measurements

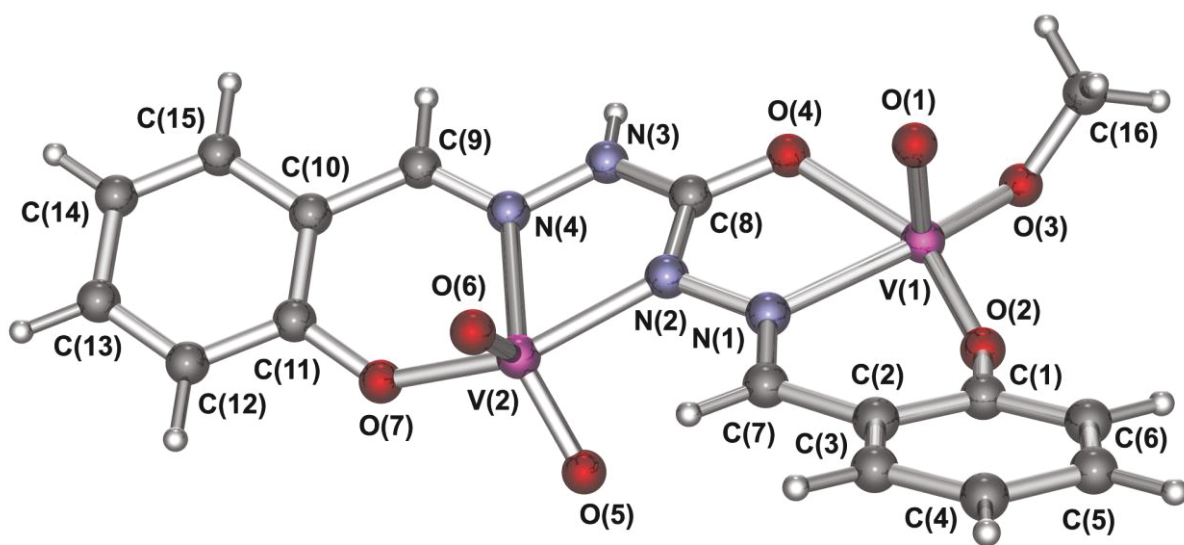
Magnetic properties of **1**, **2** and **3** compounds were investigated using MPMS-5 SQUID magnetometer measuring the static magnetization. Around 20 mg of fine powdered sample was closed in ampoule whose diamagnetic contribution was subtracted before analysis. Temperature dependence of magnetization $M(T)$ was measured in a broad temperature range (2–340 K). The overlap of susceptibility $\chi(T)$ curves measured in fields of 1T and 0.1T points to the linear magnetic response, as confirmed with measurement of $M(H)$ at several temperatures up to 5T field. Therefore, the susceptibility is a proper quantity for the analysis.

Magnetic susceptibility of all three compounds is constant with temperature and negative, i.e. the compounds are diamagnetic in the temperature interval 2–340 K. The molar susceptibilities amount $(-92\pm 8)\cdot 10^{-6}$ emu/mol, $(-91\pm 8)\cdot 10^{-6}$ emu/mol and $(-105\pm 8)\cdot 10^{-6}$ emu/mol, for compounds **1**, **2** and **3**, respectively, normalized to moles of vanadium ions. The small error of estimation comes from the unknown precise background contribution, which obviously can be neglected although the samples quantities were not too large.

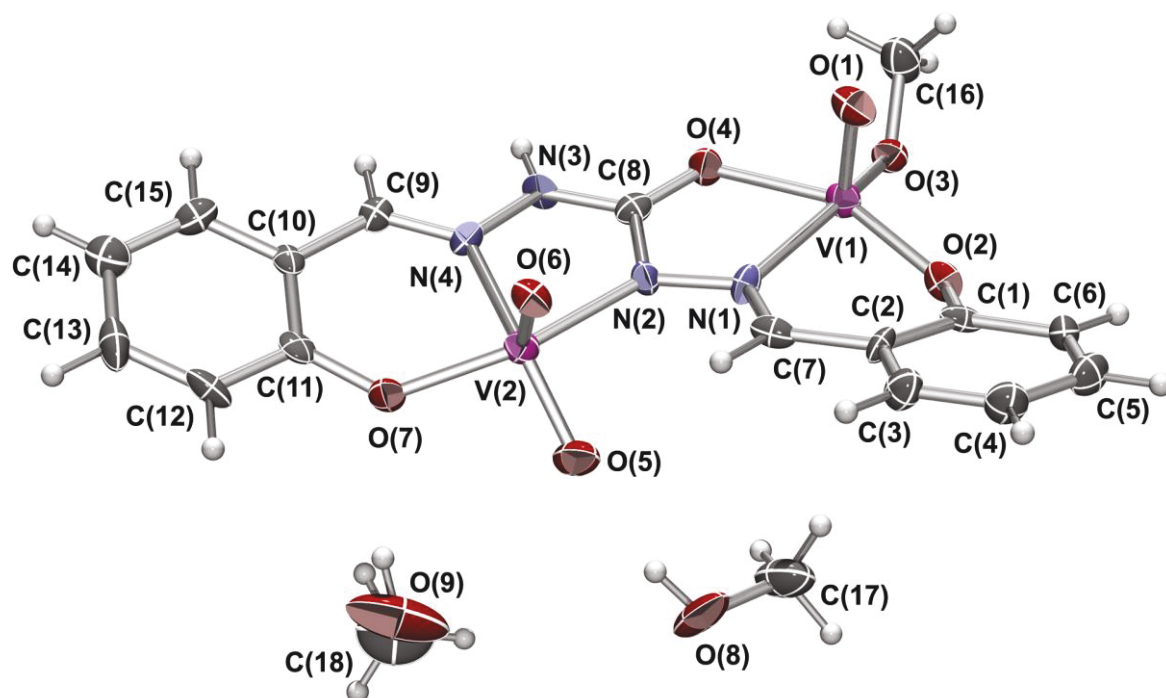
From the molar mass of the compounds, the empirical procedure for diamagnetic contribution of the formula units gives $(-130\pm 10)\cdot 10^{-6}$ emu/mol, normalized to mole of vanadium ions. The remaining part could be associated to the temperature independent paramagnetic contribution of vanadium V(v), which follows to be $(35\pm 10)\cdot 10^{-6}$ emu/mol from our results. This is of right order of magnitude if compared to other transition metals, but exact comparison is not available, since the literature is lacking with vanadium data.

Small deviations from constant $\chi(T)$ at lowest temperatures were tried to be described with paramagnetic contribution, which in compound **1** amounts less than 0.4% of paramagnetic impurities (and zero in **2** and **3**), and with dimerized units, which in **2** and **3** amount less than 1% of dimeric impurities (and zero in **1**). However, this is rather small contribution, and could be disregarded from any quantitative analysis.

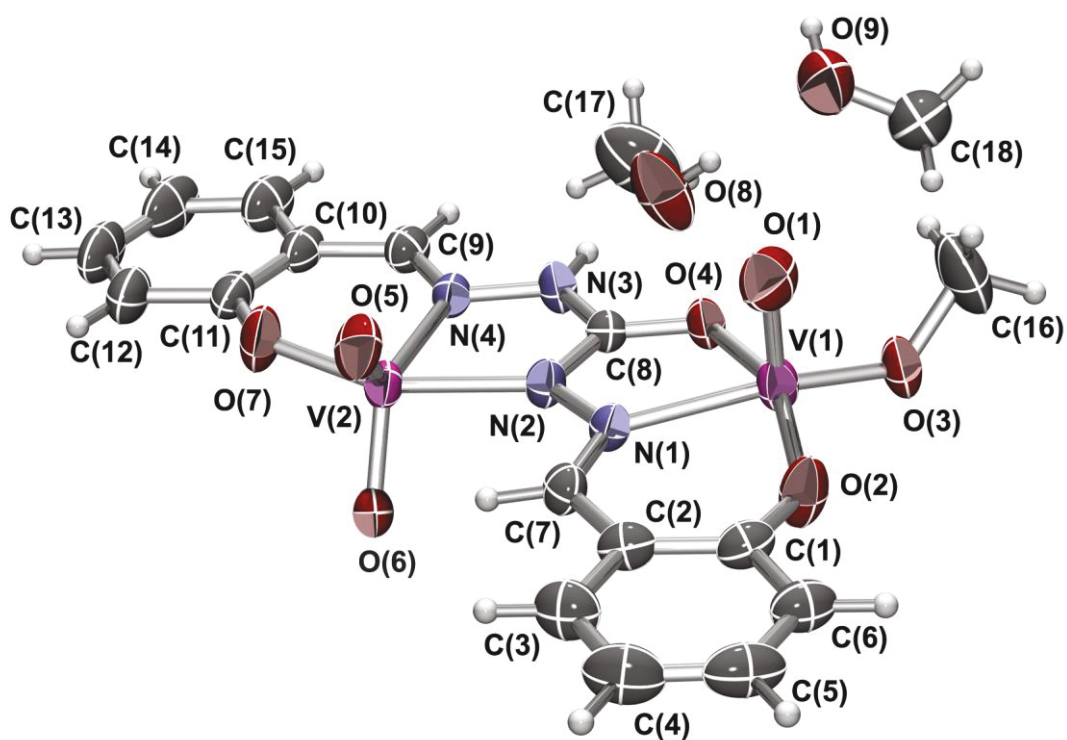
3. Molecular and crystal structures



(a)



(b)



(c)

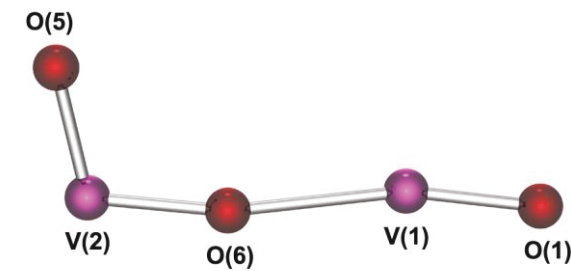
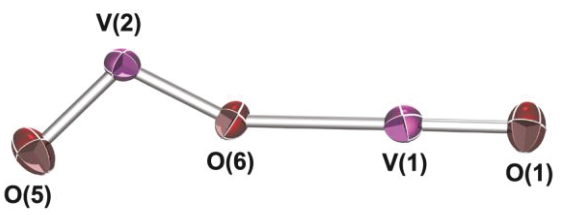
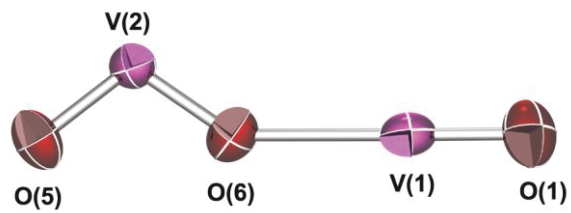
Figure S3. ORTEP POV-ray rendered view of the asymmetric units with the atom-labelling schemes of: (a) **1**, (b) **2**, and (c) **3**. The displacement ellipsoids are drawn at the 30 % probability level at 110 K (for **2**) and at 293 K (for **3**).

Table S1. Selected geometrical parameters for compounds **1**, **2**, and **3**.

A-B-C	$d(\text{A-B})/\text{\AA}$	$d(\text{B-C})/\text{\AA}$	$\angle(\text{A-B-C})/^\circ$	$d(\text{A-B})/\text{\AA}$	$d(\text{B-C})/\text{\AA}$	$\angle(\text{A-B-C})/^\circ$	$d(\text{A-B})/\text{\AA}$	$d(\text{B-C})/\text{\AA}$	$\angle(\text{A-B-C})/^\circ$
	1			2			3		
O(1)-V(1)-O(2)	1.582(3)	1.646(3)	104.23(14)	1.572(4)	1.840(4)	100.53(17)	1.5878(17)	1.8297(18)	100.73(10)
O(1)-V(1)-O(3)	1.582(3)	1.692(2)	100.01(14)	1.572(4)	1.755(3)	103.46(17)	1.5878(17)	1.7399(17)	102.55(9)
O(1)-V(1)-O(4)	1.582(3)	2.0584(19)	80.97(13)	1.572(4)	2.005(4)	94.90(17)	1.5878(17)	1.9853(16)	97.03(9)
O(1)-V(1)-N(1)	1.582(3)	2.173(2)	87.79(13)	1.572(4)	2.129(4)	95.32(18)	1.5878(17)	2.1526(19)	93.97(9)
O(2)-V(1)-O(3)	1.646(3)	1.692(2)	106.68(13)	1.840(4)	1.755(3)	104.23(15)	1.8297(18)	1.7399(17)	103.28(8)
O(2)-V(1)-N(1)	1.646(3)	2.173(2)	82.60(11)	1.840(4)	2.129(4)	84.88(16)	1.8297(18)	2.1526(19)	84.96(7)
O(2)-V(1)-O(4)	1.646(3)	2.0584(19)	152.98(12)	1.840(4)	2.005(4)	155.15(16)	1.8297(18)	1.9853(16)	154.01(8)
N(1)-V(1)-O(3)	2.173(2)	1.692(2)	165.75(10)	2.129(4)	1.755(3)	157.04(17)	2.1526(19)	1.7399(17)	159.65(8)
N(1)-V(1)-O(4)	2.173(2)	2.0584(19)	71.00(7)	2.129(4)	2.005(4)	74.33(16)	2.1526(19)	1.9853(16)	74.97(7)
O(3)-V(1)-O(4)	1.692(2)	2.0584(19)	98.27(9)	1.755(3)	2.005(4)	90.80(15)	1.7399(17)	1.9853(16)	91.10(7)
V(1)-O(3)-C(16)	1.692(2)	1.379(2)	124.89(13)	1.755(3)	1.413(6)	129.9(3)	1.7399(17)	1.422(4)	128.97(19)
O(2)-C(1)-C(2)	1.267(3)	1.4003(18)	120.00(15)	1.365(6)	1.384(7)	121.3(5)	1.323(3)	1.410(4)	121.8(2)
C(1)-C(2)-C(7)	1.4003(18)	1.4854(17)	119.71(11)	1.384(7)	1.452(8)	122.4(5)	1.410(4)	1.450(4)	122.9(2)
C(2)-C(7)-N(1)	1.4854(17)	1.336(2)	121.20(13)	1.452(8)	1.281(7)	124.5(5)	1.450(4)	1.288(3)	123.3(2)
N(1)-N(2)-C(8)	1.420(2)	1.3301(19)	109.72(15)	1.375(6)	1.347(7)	109.6(4)	1.394(3)	1.330(3)	108.93(18)
N(2)-C(8)-O(4)	1.3301(19)	1.2826(18)	119.54(13)	1.347(7)	1.262(6)	122.5(5)	1.330(3)	1.272(3)	124.7(2)
N(2)-C(8)-N(3)	1.3301(19)	1.3838(14)	117.17(11)	1.347(7)	1.331(7)	115.4(5)	1.330(3)	1.339(3)	115.9(2)
C(8)-N(3)-N(4)	1.3838(14)	1.3692(12)	114.02(8)	1.331(7)	1.387(6)	115.7(4)	1.339(3)	1.385(3)	115.4(2)
N(3)-N(4)-C(9)	1.3692(12)	1.3012(16)	120.13(9)	1.387(6)	1.280(7)	117.9(4)	1.385(3)	1.291(3)	115.7(2)
N(4)-C(9)-C(10)	1.3012(16)	1.4688(18)	123.58(11)	1.280(7)	1.456(7)	123.8(5)	1.291(3)	1.417(4)	125.0(2)
C(9)-C(10)-C(11)	1.4688(18)	1.4143(17)	121.36(12)	1.456(7)	1.392(8)	121.0(5)	1.417(4)	1.396(4)	121.3(3)
C(10)-C(11)-O(7)	1.4143(17)	1.337(3)	120.77(13)	1.392(8)	1.341(7)	122.4(5)	1.396(4)	1.327(4)	122.1(2)
O(5)-V(2)-O(6)	1.578(4)	1.6477(16)	106.1(2)	1.621(3)	1.618(4)	108.98(18)	1.6174(18)	1.6208(17)	107.92(9)
O(5)-V(2)-O(7)	1.578(4)	1.868(3)	108.2(3)	1.621(3)	1.876(4)	96.63(17)	1.6174(18)	1.8788(18)	99.48(9)
O(5)-V(2)-N(2)	1.578(4)	2.007(2)	88.8(2)	1.621(3)	2.046(4)	92.48(17)	1.6174(18)	2.0635(19)	92.43(8)
O(5)-V(2)-N(4)	1.578(4)	2.2605(18)	136.7(2)	1.621(3)	2.167(4)	138.36(16)	1.6174(18)	2.171(2)	128.22(8)
O(6)-V(2)-O(7)	1.6477(16)	1.868(3)	98.07(12)	1.618(4)	1.876(4)	105.25(17)	1.6208(17)	1.8788(18)	103.10(8)
O(6)-V(2)-N(2)	1.6477(16)	2.007(2)	98.38(9)	1.618(4)	2.046(4)	97.24(18)	1.6208(17)	2.0635(19)	95.38(8)
O(6)-V(2)-N(4)	1.6477(16)	2.2605(18)	115.13(9)	1.618(4)	2.167(4)	111.48(17)	1.6208(17)	2.171(2)	122.45(8)
O(7)-V(2)-N(4)	1.868(3)	2.2605(18)	79.28(8)	1.876(4)	2.167(4)	82.06(16)	1.8788(18)	2.171(2)	81.27(8)
O(7)-V(2)-N(2)	1.868(3)	2.007(2)	151.87(12)	1.876(4)	2.046(4)	151.37(17)	1.8788(18)	2.0635(19)	153.61(8)
N(2)-V(2)-N(4)	2.007(2)	2.2605(18)	73.11(8)	2.046(4)	2.167(4)	73.24(17)	2.0635(19)	2.171(2)	72.90(8)

3.1. $[\text{V}_2\text{O}_3]^{4+}$ core configuration

Table S2. Selected geometrical parameters for $[\text{V}_2\text{O}_3]^{4+}$ units in compounds **1**, **2**, and **3**

Compound		Selected angle values and bond distances
1		$\angle \text{V}(2)\text{--O}(6)\text{--V}(1)$ $161.4(1)^\circ$ $\text{O}(5)=\text{V}(2)\dots\text{V}(1)=\text{O}(1)$ $\text{V}(1)\text{--O}(1)$ $1.582(3)$ Å $\text{V}(1)\text{--O}(6)$ $2.145(2)$ Å $\text{V}(2)\text{--O}(5)$ $1.578(4)$ Å $\text{V}(2)\text{--O}(6)$ $1.6477(16)$ Å
2		$\angle \text{V}(2)\text{--O}(6)\text{--V}(1)$ $148.8(2)^\circ$ $\text{O}(5)=\text{V}(2)\dots\text{V}(1)=\text{O}(1)$ $\text{V}(1)\text{--O}(1)$ $1.572(4)$ Å $\text{V}(1)\text{--O}(6)$ $2.290(3)$ Å $\text{V}(2)\text{--O}(5)$ $1.621(3)$ Å $\text{V}(2)\text{--O}(6)$ $1.618(4)$ Å
3		$\angle \text{V}(2)\text{--O}(6)\text{--V}(1)$ $145.2(1)^\circ$ $\text{O}(5)=\text{V}(2)\dots\text{V}(1)=\text{O}(1)$ $\text{V}(1)\text{--O}(1)$ $1.588(2)$ Å $\text{V}(1)\text{--O}(6)$ $2.341(2)$ Å $\text{V}(2)\text{--O}(5)$ $1.6174(18)$ Å $\text{V}(2)\text{--O}(6)$ $1.6208(17)$ Å

In all here presented structures O(6) oxygen atom bridges vanadium V(1) and V(2) atoms in unsymmetrical fashion, with very short V(2)–O(6) bond and very long V(1)–O(6) bond. Such asymmetry is due to the *trans* location of the bridging O(6) atom with respect to the terminal O(1) atom.

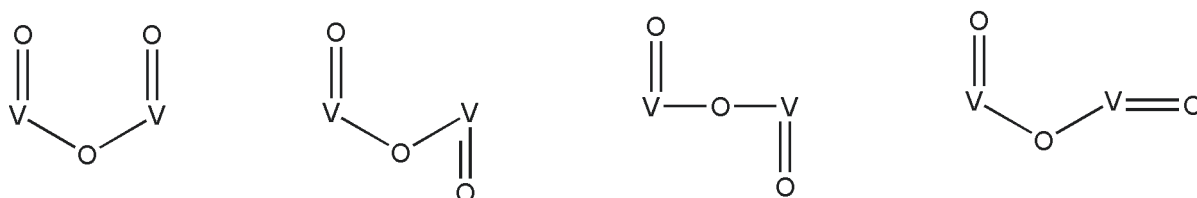
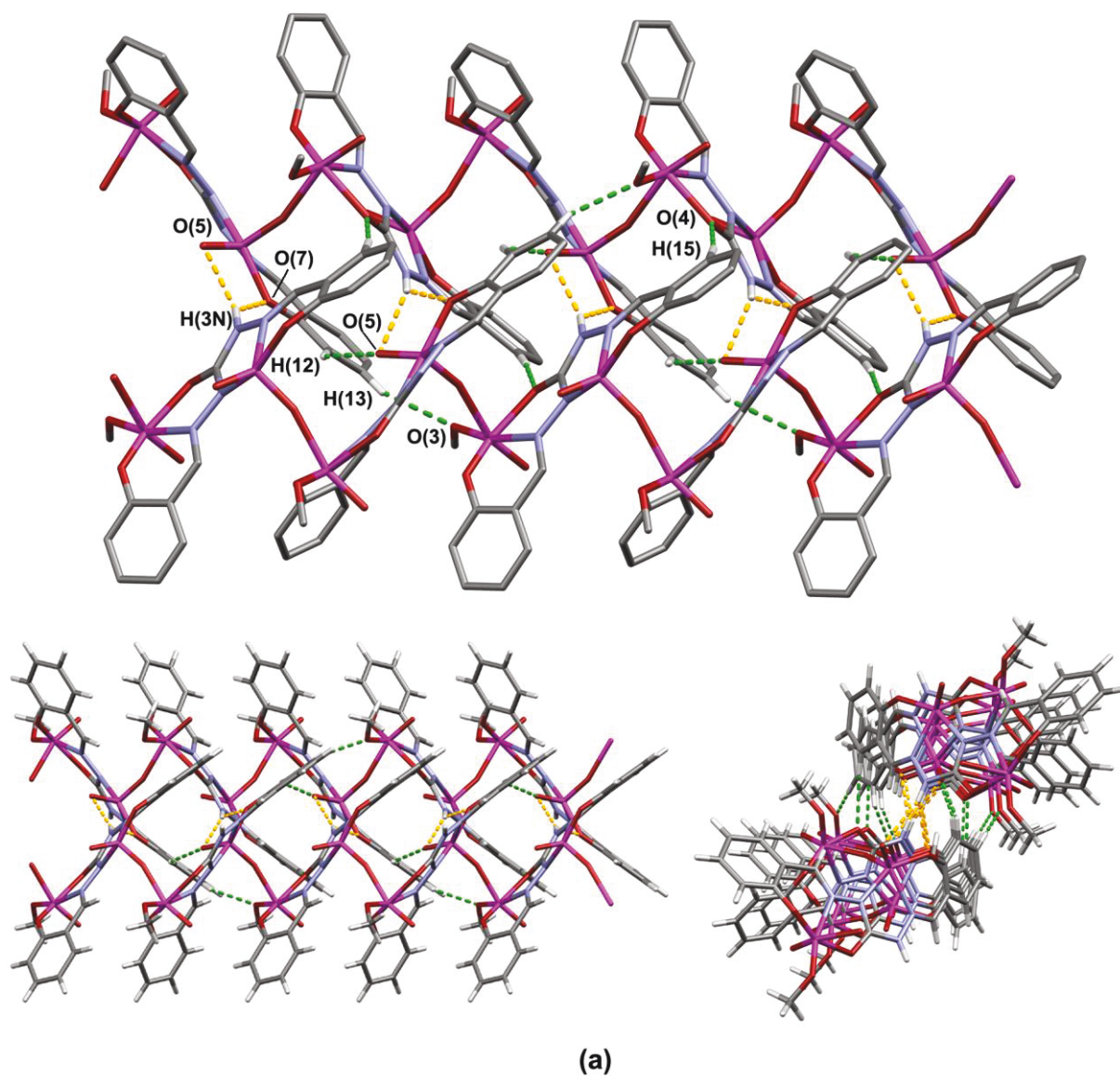
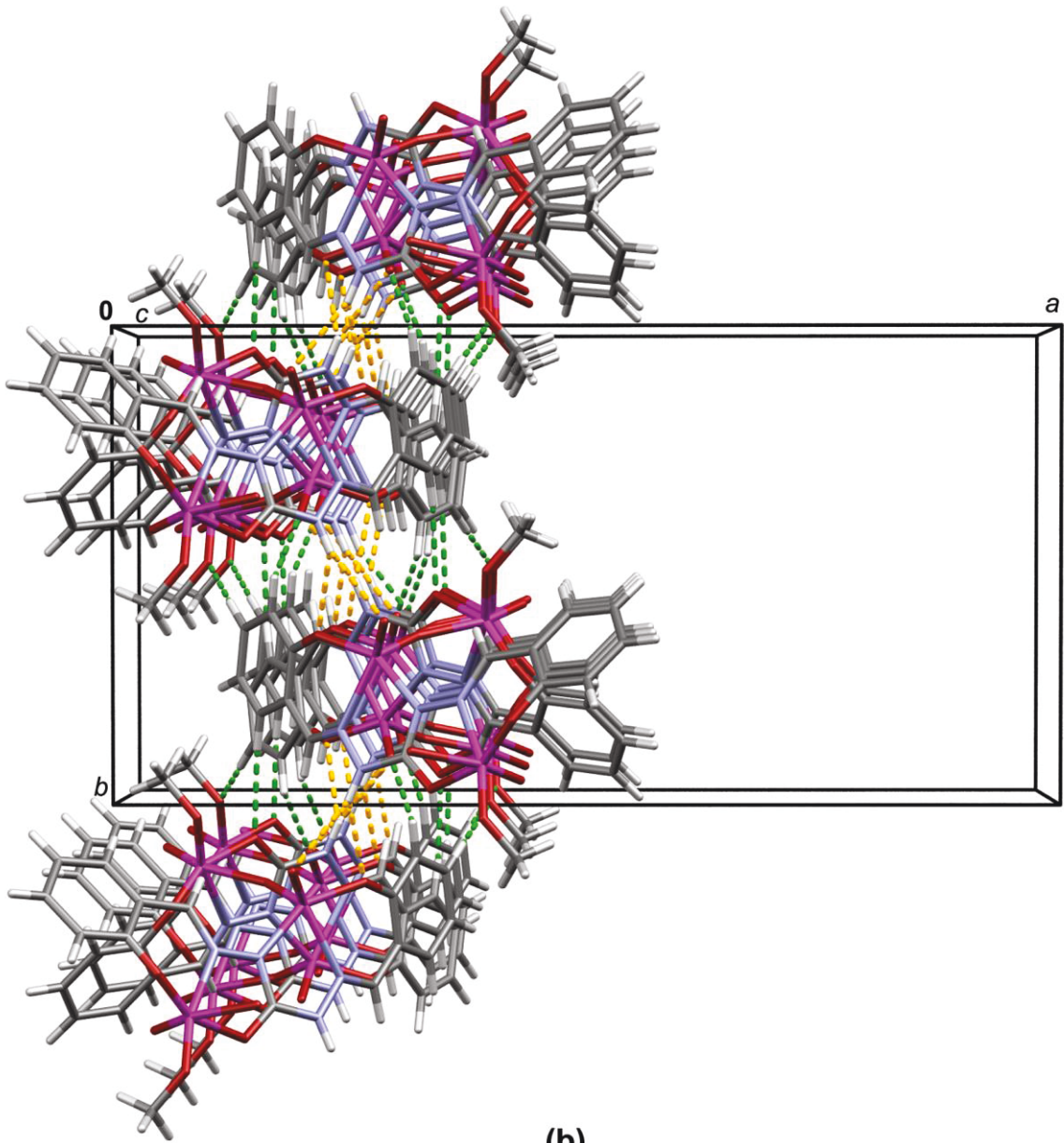


Figure S4. Possible configurations of $[\text{V}_2\text{O}_3]^{n+}$ core ($n = 2, 3, 4$): (a) *syn*-angular; (b) *anti*-angular; (c) *anti*-linear, and (d) *twist*-angular.

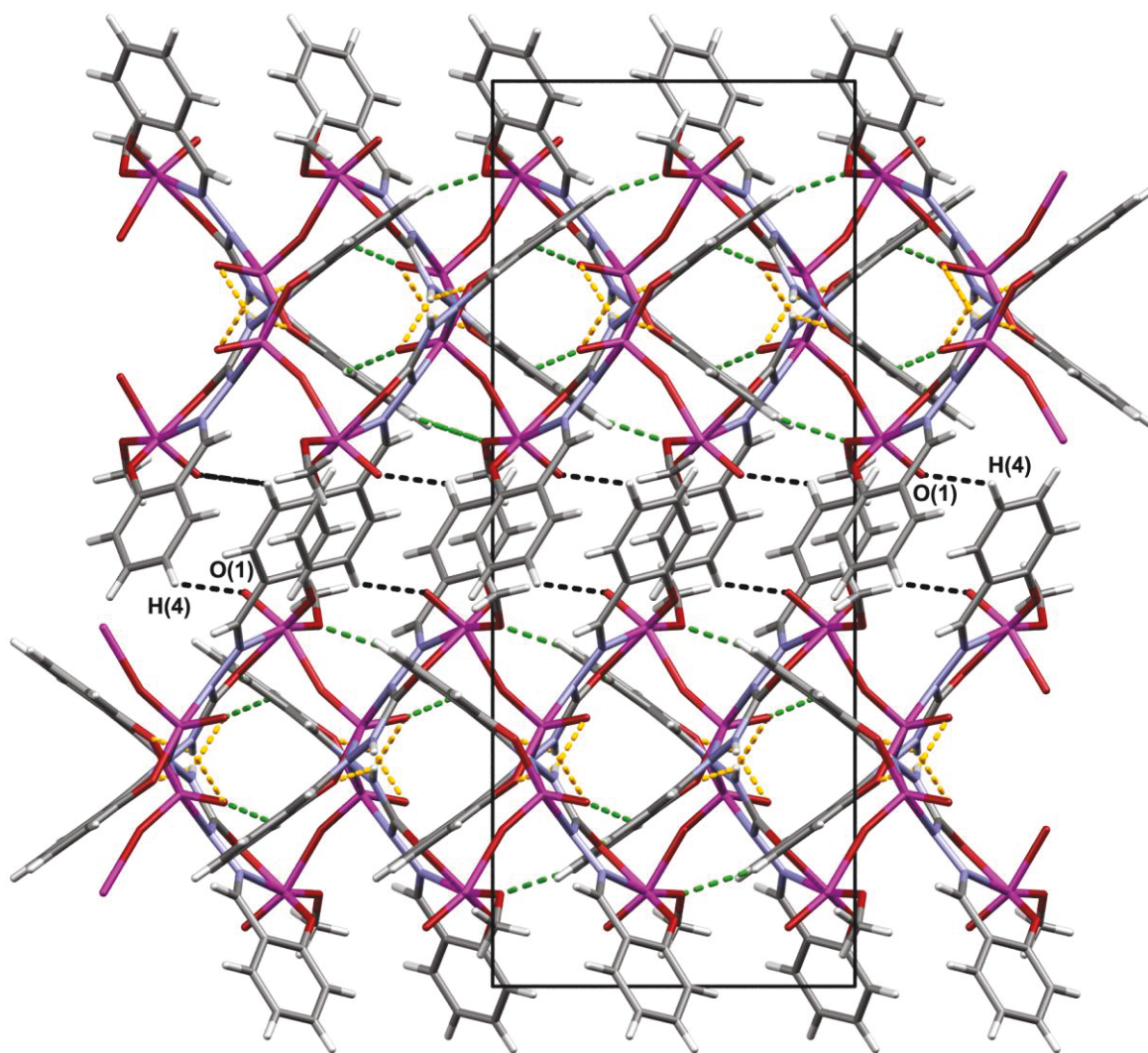
The configuration of the $V_2O_3^{n+}$ core ($n = 2, 3, 4$) largely depends on the coordination environment about vanadium atoms. If both vanadium centers assume square pyramidal geometry the core adopts *syn*-angular (Figure S4(a)) or *anti*-angular (Figure S4(b)) configuration. In contrast, if both atoms have octahedrally shaped environment the core usually adopts *anti*-linear configuration (Figure S4(c)). In the case of unsymmetrical coordination geometry configuration of the core is often somewhere in between that characteristic for bis-octahedral and bis-square pyramidal environment, best described by *twist*-angular configuration. The $V(2)-O(6)-V(1)$ angle values along with the $O(5)=V(2)...V(1)=O(1)$ torsion angle values, for here described structures, indicate *twist*-angular configuration of the $V_2O_3^{4+}$ core for **1**, and *anti*-angular configuration for those found in **2** and **3**.

3.2. Crystal structures





(b)



(c)

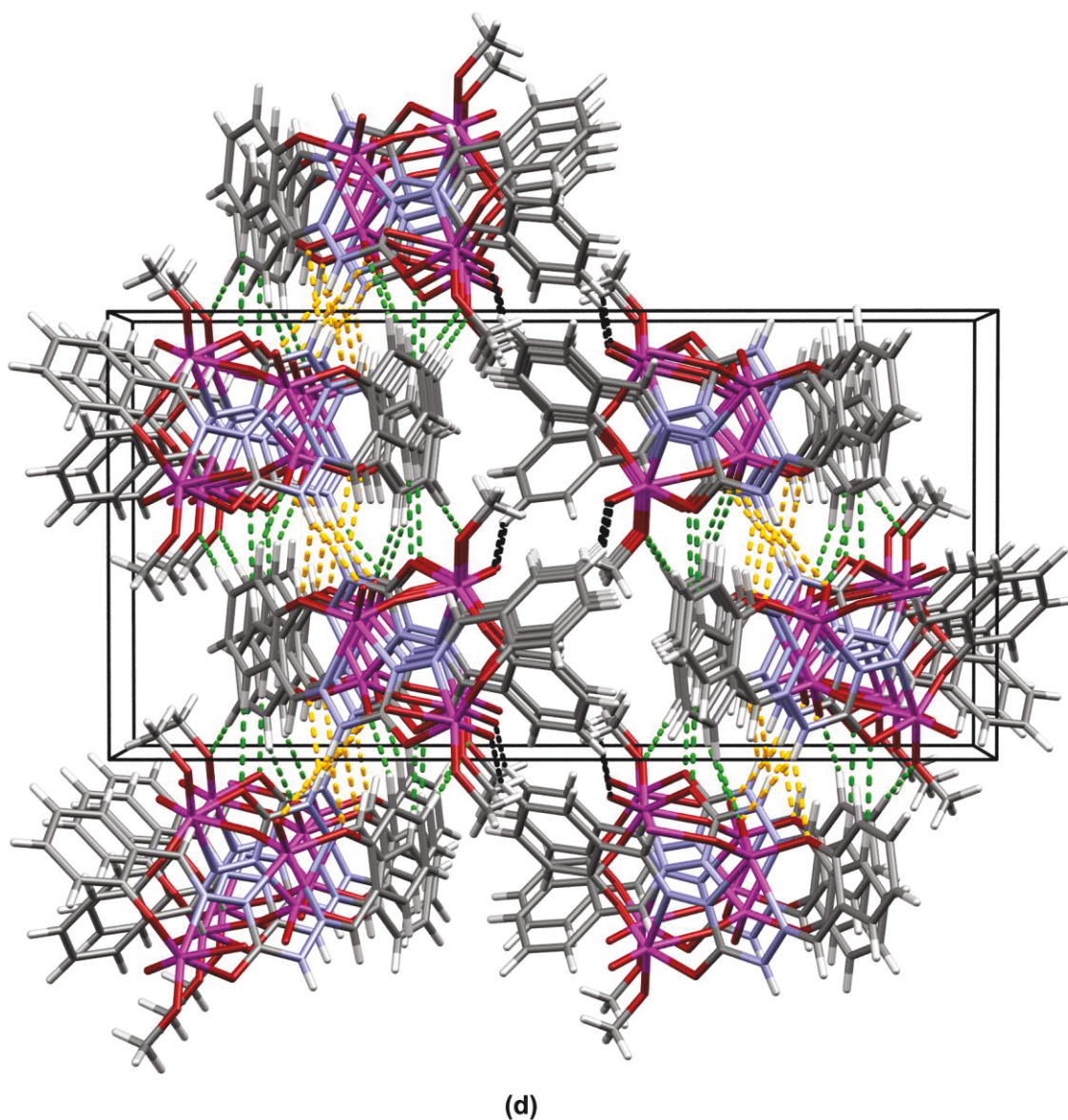
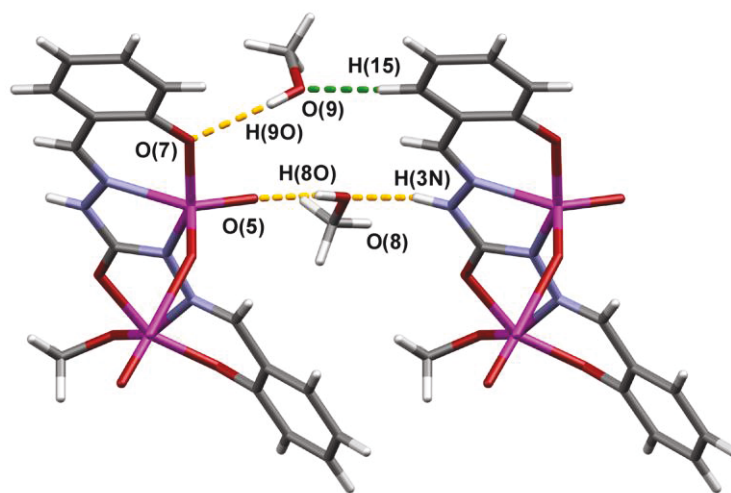
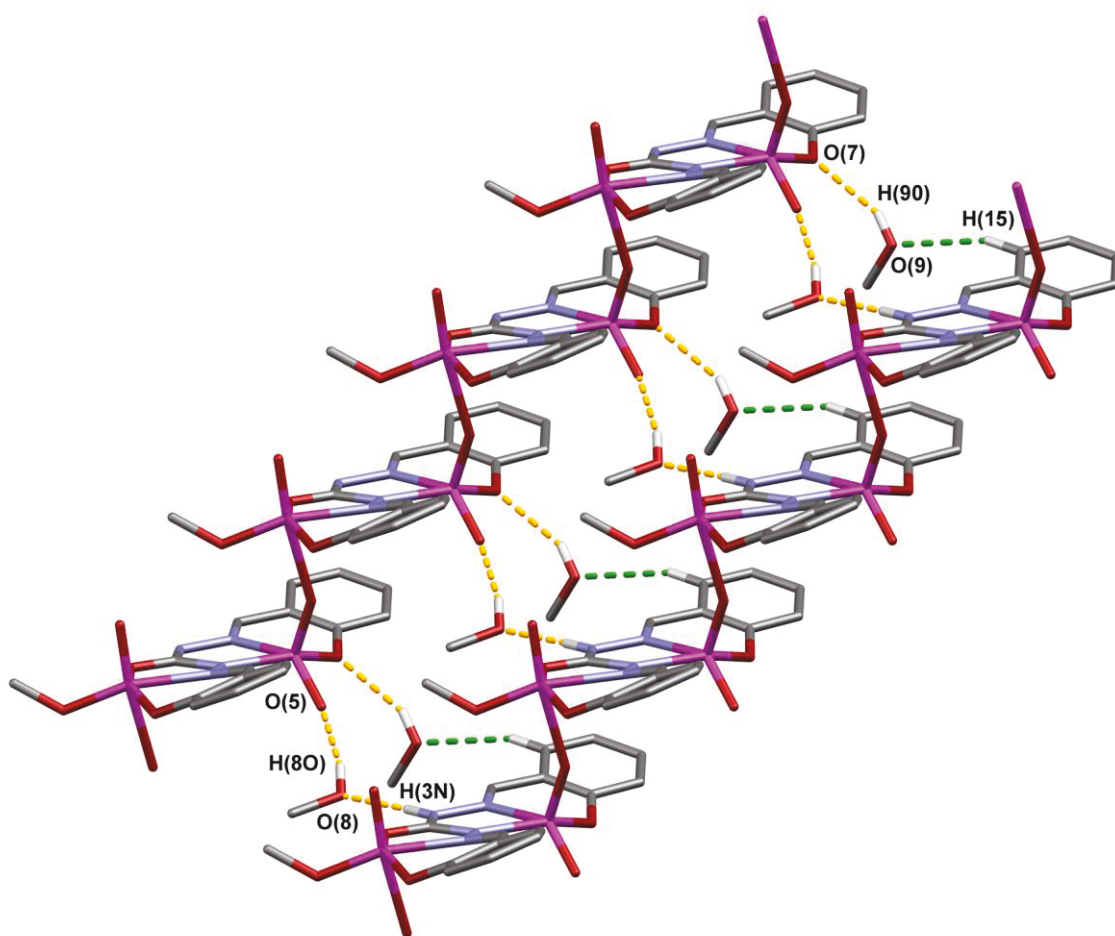
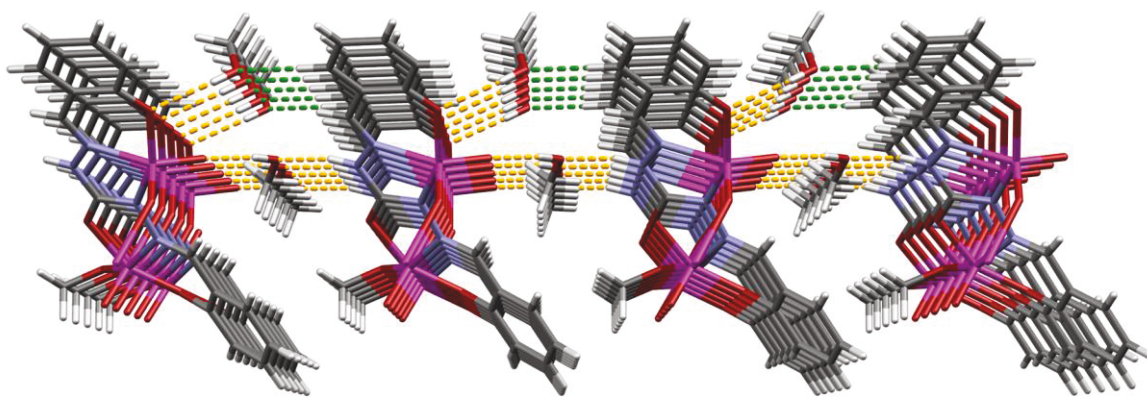


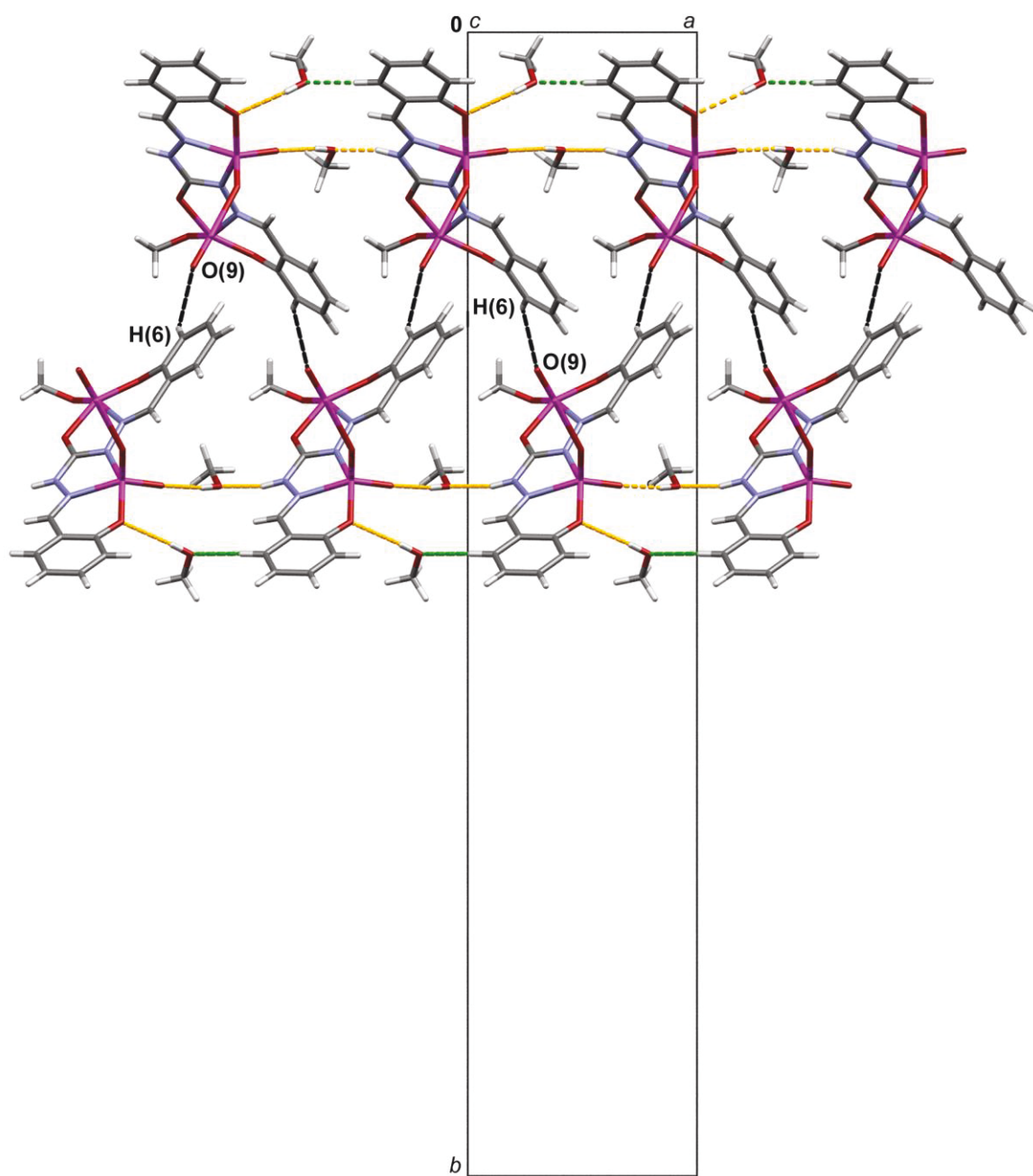
Figure S5. Packing diagrams for **1**. Infinite chains in **1** are mutually assembled *via* N–H···O (orange dashed lines) and C–H···O (green dashed lines) interactions into layers parallel to the *bc*-plane (Table Sx). Neighboring layers are joined through C–H···O (black dashed line) interaction into the final three-dimensional architecture. (a) Two infinite chains assembled *via* N(3)–H(3N)···O(5), N(3)–H(3N)···O(7) (orange dashed lines) and C(12)–H(12)···O(5), C(13)–H(13)···O(3) and C(15)–H(15)···O(4) (green dashed lines). Hydrogen atoms not involved in the abovementioned interactions are not presented for clarity (upper figure). View on two chains down the *b*-axis (bellow left) and down the *c*-axis (bellow right). (b) Part of the layer parallel to the *bc*-plane (view down the *c*-axis). In (c) and (d) two layers are joined through C(4)–H(4)···O(1) (black dashed line). (c) View down the *b*-axis and (d) view down the *c*-axis.



(a)

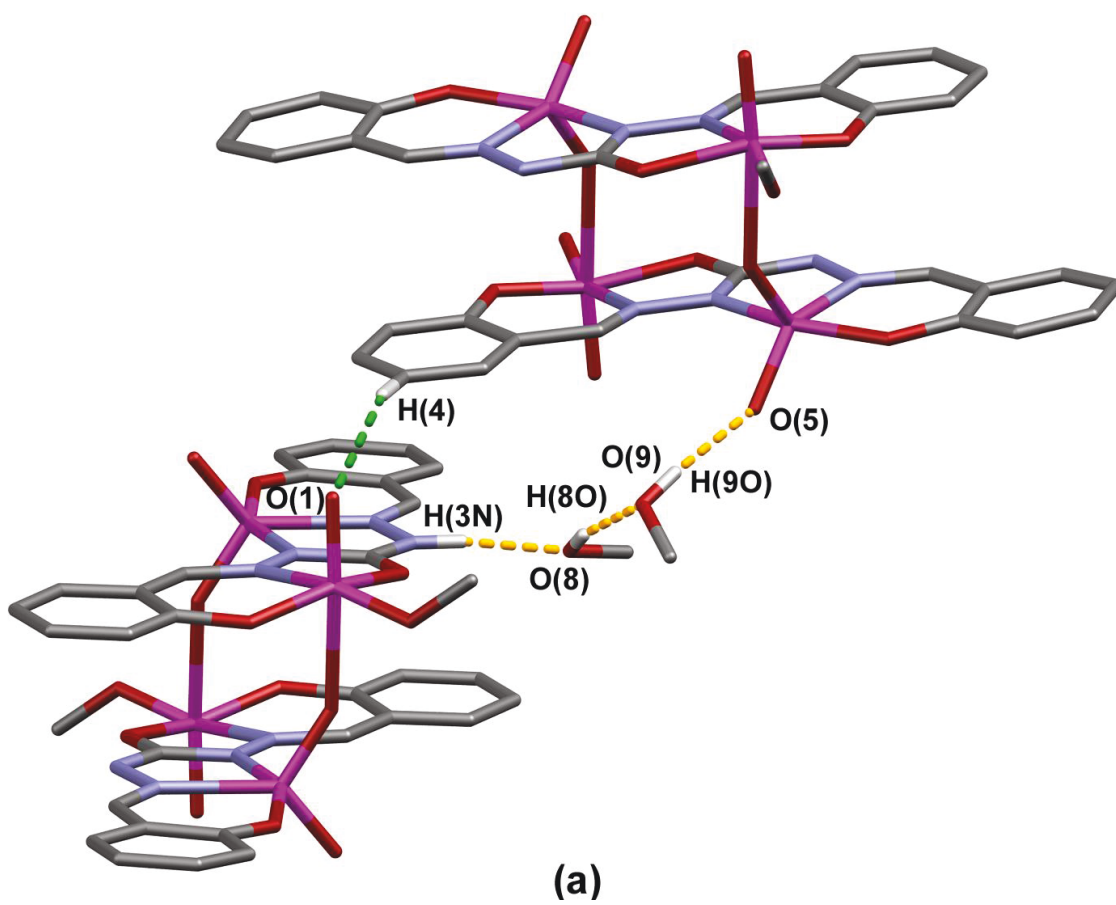


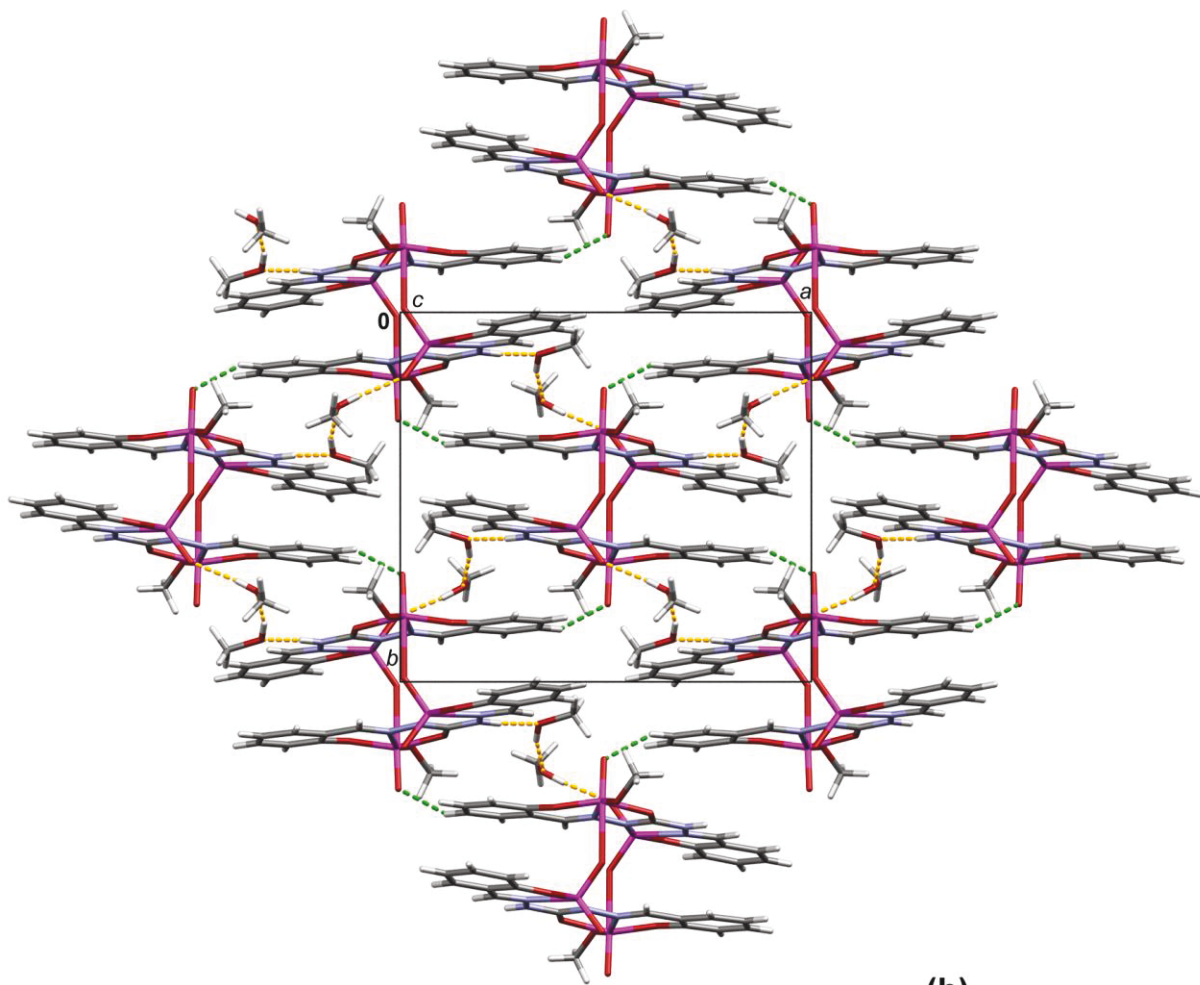
(b)



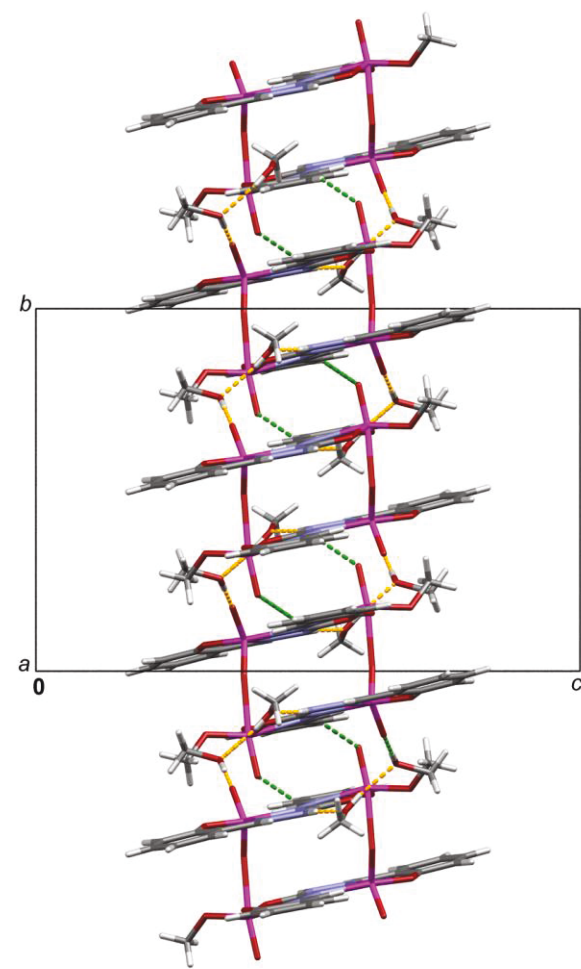
(c)

Figure S6. Packing diagrams for **2**. Infinite chains in **2** are mutually joined *via* methanol molecules by N–H...O, O–H...O (orange dashed lines) and C–H...O (green dashed lines) interactions into layers parallel to the *ac*-plane (Table S3). Neighboring layers are joined through C–H...O (black dashed line) interactions into the three-dimensional architecture. (a) Two Infinite chains in **2** are mutually joined *via* methanol molecules by N(3)–H(3N)...O(8), O(8)–H(8O)...O(5), O(9)–H(9O)...O(7) (orange dashed lines) and C(15)–H(15)...O(9) (green dashed lines) interactions into layers parallel to the *ac*-plane. The hydrogen atoms which are not involved in the abovementioned interactions are not presented for clarity (upper figure). View on two chains down the *c*-axis (figure below). (b) Part of the layer parallel to the *ac*-plane (view down the *c*-axis). (c) Adjacent layers are joined through C(6)–H(6)...O(1) interactions (black dashed line). In (c) molecules are viewed down the *c*.





(b)



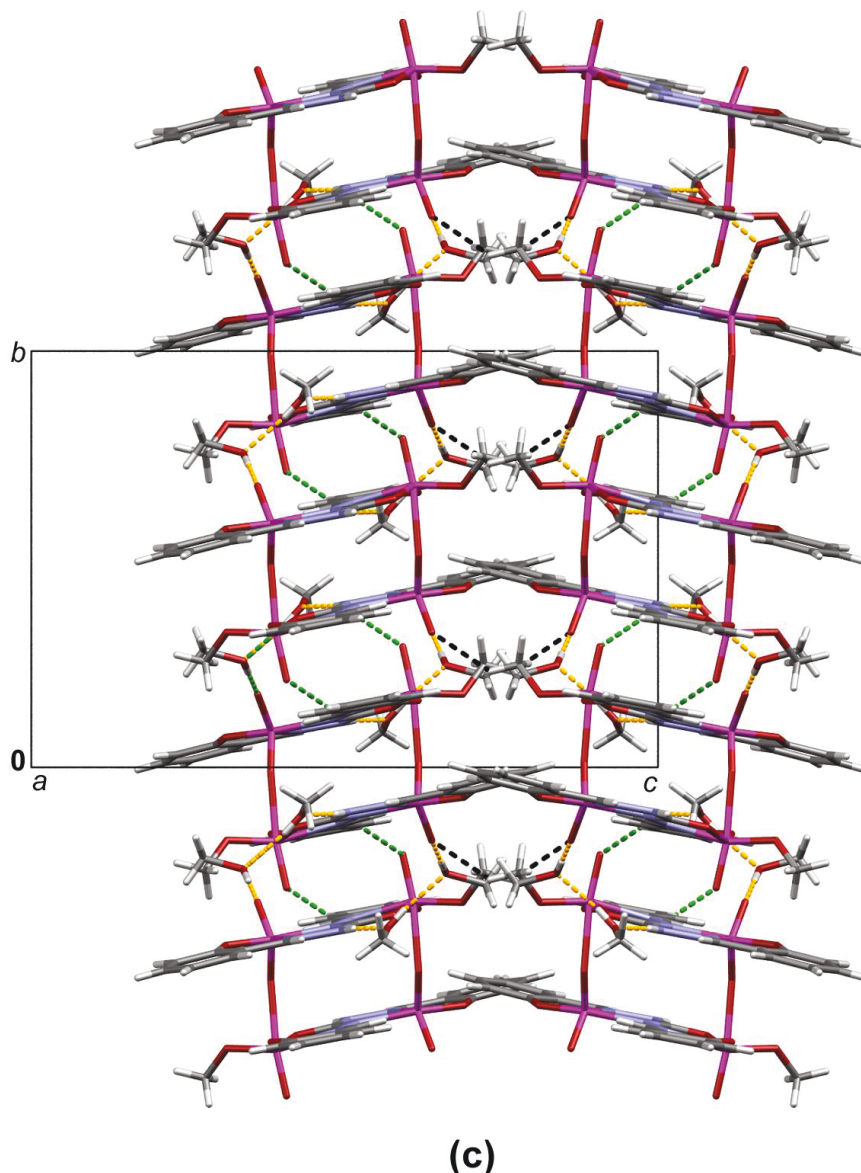


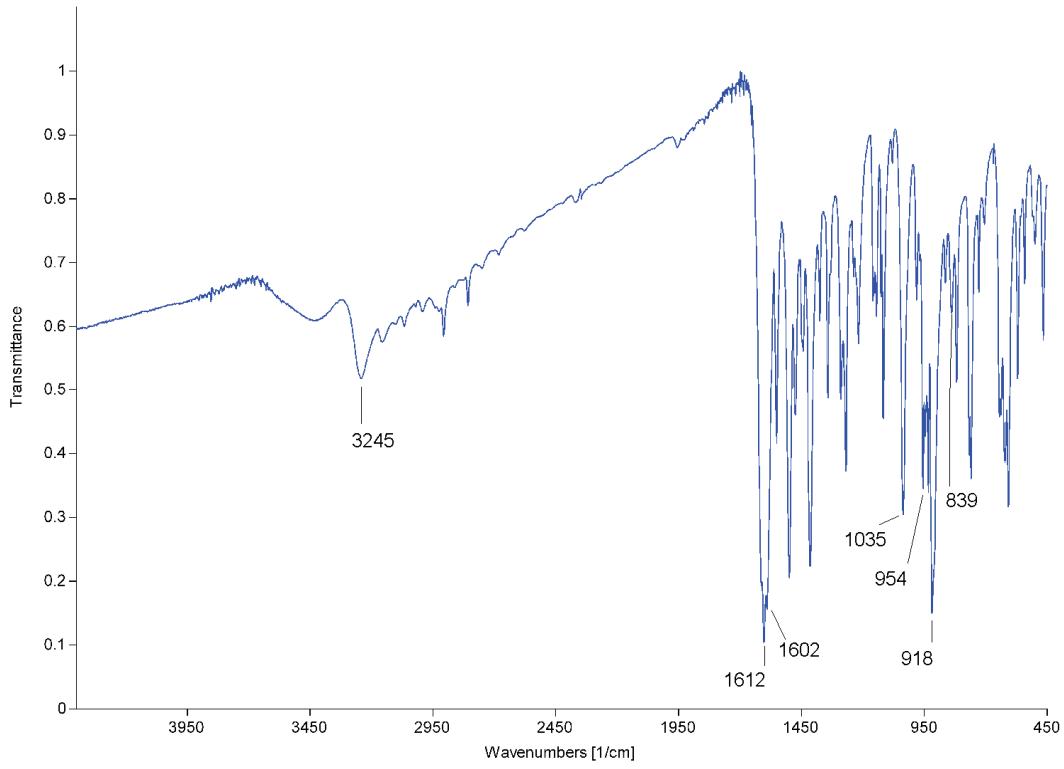
Figure S7. Packing diagram for **3**. Discrete tetranuclear units are joined *via* methanol molecules by N–H...O, O–H...O (orange dashed lines) and C–H...O (green dashed lines) interactions into layers parallel to the *ab*-plane (Table S2). Neighboring layers are joined through C–H...O (black dashed line) interactions into the three-dimensional architecture. (a) Two discrete tetranuclear units are mutually joined *via* methanol molecules by N(3)–H(3N)...O(8), O(8)–H(8O)...O(9), O(9)–H(9O)...O(5) (orange dashed lines) and C(4)–H(4)...O(1) (green dashed lines) interactions into layers parallel to the *ab*-plane. Those hydrogen atoms not involved in the abovementioned interactions are not presented for clarity. (b) Part of the layer parallel to the *ab*-plane: view down the *c*-axis (left) and view down the *a*-axis (right). (c) Adjacent layers are joined through C(16)–H(16B)...O(5) interactions (black dashed line). In (c) molecules are viewed down the *a*-axis.

Table S3. Intermolecular interactions found in the structures **1**, **2** and **3**

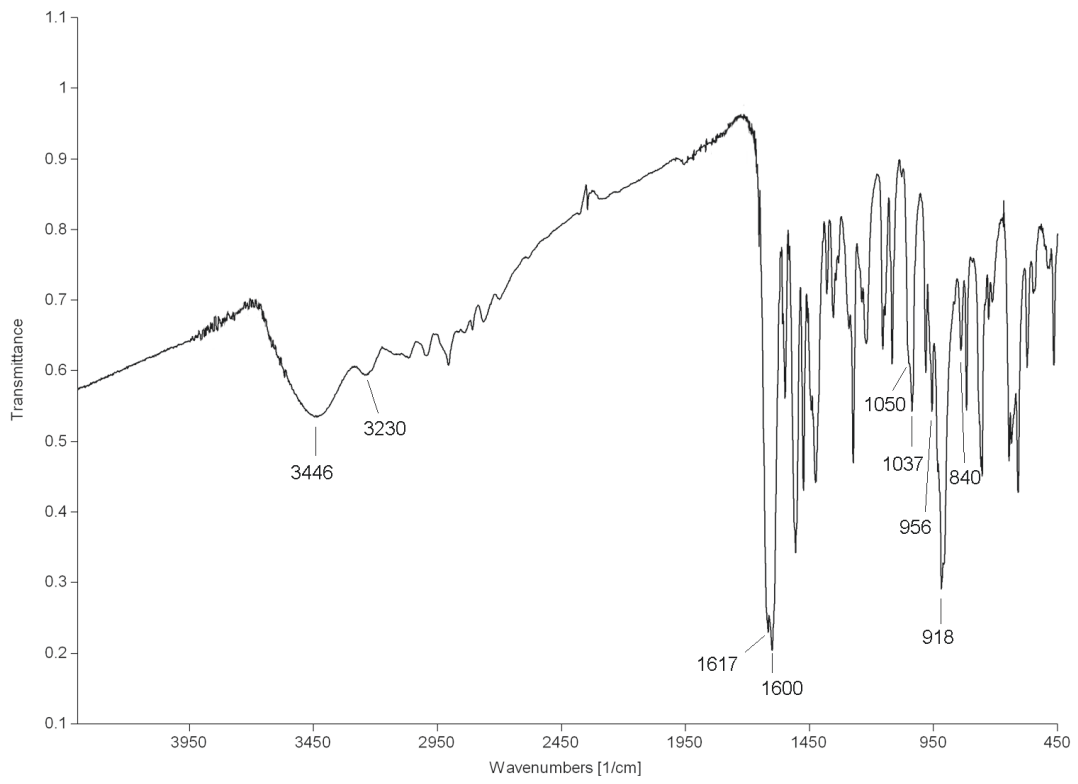
D–H...A	D–H	H...A	D...A	\angle D–H...A	Symmetry code
1					
N(3)–H(3N)...O(5)	0.879(7)	2.535(9)	3.356(5)	155.8(6)	$1/2-x, 1/2+y, z$
N(3)–H(3N)...O(7)	0.879(7)	2.564(7)	3.266(2)	137.5(6)	$1/2-x, 1/2+y, z$
C(12)–H(12)...O(5)	0.985(5)	2.405(8)	3.091(4)	126.2(6)	$1/2-x, 1-y, 1/2+z$
C(13)–H(13)...O(3)	1.001(5)	2.505(6)	3.451(2)	157.5(4)	$1/2-x, -1/2+y, 1+z$
C(15)–H(15)...O(4)	0.984(5)	2.462(5)	3.4334(18)	169.2(4)	$1/2-x, 2-y, 1/2+z$
C(4)–H(4)...O(1)	1.011(5)	2.495(7)	3.267(3)	132.8(4)	$1-x, -1/2+y, 1/2-z$
2					
N(3)–H(3N)...O(8)	0.87(3)	1.85(3)	2.696(6)	164(4)	$-1+x, y, z$
O(8)–H(8O)...O(5)	0.86(4)	1.83(4)	2.679(5)	167(4)	–
O(9)–H(9O)...O(7)	0.84(6)	2.15(6)	2.931(6)	155(7)	–
C(15)–H(15)...O(9)	0.9500	2.4900	3.394(7)	158.00	$-1+x, y, z$
C(6)–H(6)...O(1)	0.9500	2.662(3)	3.354(6)	130.1(3)	$1/2+x, 1/2-y, 1/2+z$
3					
N(3)–H(3N)...O(8)	0.85(2)	1.89(2)	2.733(3)	173(2)	–
O(8)–H(8O)...O(9)	0.82(3)	1.89(3)	2.677(4)	164(3)	–
O(9)–H(9O)...O(5)	0.84(3)	1.94(3)	2.775(3)	175(4)	$1/2+x, 1/2-y, 1-z$
C(4)–H(4)...O(1)	0.9500	2.5000	3.374(4)	153.00	$-1/2+x, 1/2-y, 1-z$
C(16)–H(16B)...O(5)	0.9800	2.5600	3.256(4)	128.00	$x, 1/2-y, 1/2+z$

4. IR spectroscopy

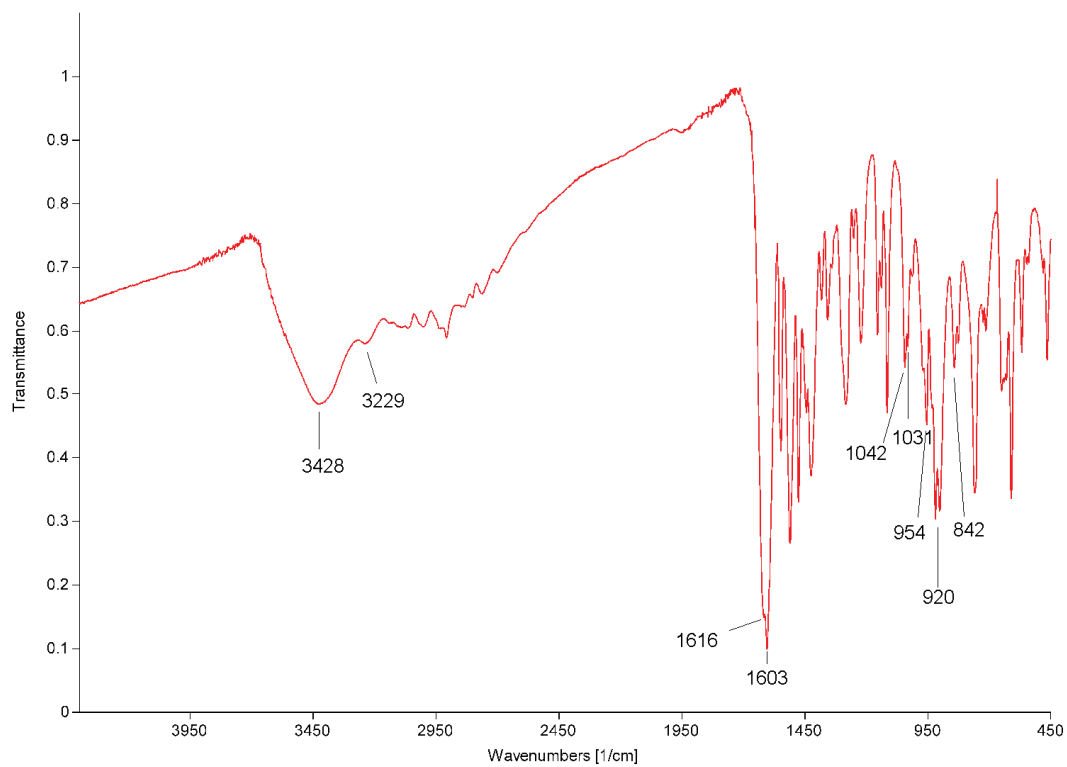
IR spectra of complexes **1–3** are quite similar, with the strong band positioned, in all cases, between 3230 and 3240 cm^{-1} , which is attributed to N–H stretching. The same band is observed at 3267 cm^{-1} in the spectrum of free ligand. Additional broad band at ≈ 3400 cm^{-1} , in the spectra of both $\{[\text{V}_2\text{O}_3(\text{HL})(\text{OCH}_3)] \cdot 2\text{CH}_3\text{OH}\}_n$ (**2**) and $[\text{V}_2\text{O}_3(\text{HL})(\text{OCH}_3)]_2 \cdot 4\text{CH}_3\text{OH}$ (**3**), is addressed to O–H stretching of crystallization methanol molecules. The band associated with C=O stretch and observed at 1715 cm^{-1} for the ligand, disappears in the spectra of all complexes, while the additional bands appear at ~ 1600 cm^{-1} due to $\nu(\text{C}=\text{N})$. This clearly indicates coordination of the ligand in its enolic form. Involvement of phenolic oxygen atoms in coordination is indicated by the shift of $\nu(\text{C}-\text{O})$ from 1267 cm^{-1} to lower wavenumbers by ~ 40 cm^{-1} . Spectrum of $\{[\text{V}_2\text{O}_3(\text{HL})(\text{OCH}_3)]\}_n$ (**1**) is characterized by the presence of a single sharp band positioned at 1035 cm^{-1} corresponding to $\nu(\text{C}-\text{O})$ of the methoxo ligand. This band is, in the case of **2** and **3**, split with the corresponding maxima at 1050 cm^{-1} , 1037 cm^{-1} (for **2**) and 1042 cm^{-1} , 1031 cm^{-1} (for **3**), which is attributed to presence of both methoxo ligand and methanol molecules. Bands addressed to V=O stretching appear at 954 cm^{-1} and 918 cm^{-1} for **1**, 956 and 918 cm^{-1} for **2**, and 954 cm^{-1} , 920 cm^{-1} for **3**. The bands corresponding to the antisymmetric V–O–V bridge vibration are observed around 840 cm^{-1} for all three compounds.



(a)



(b)



(c)

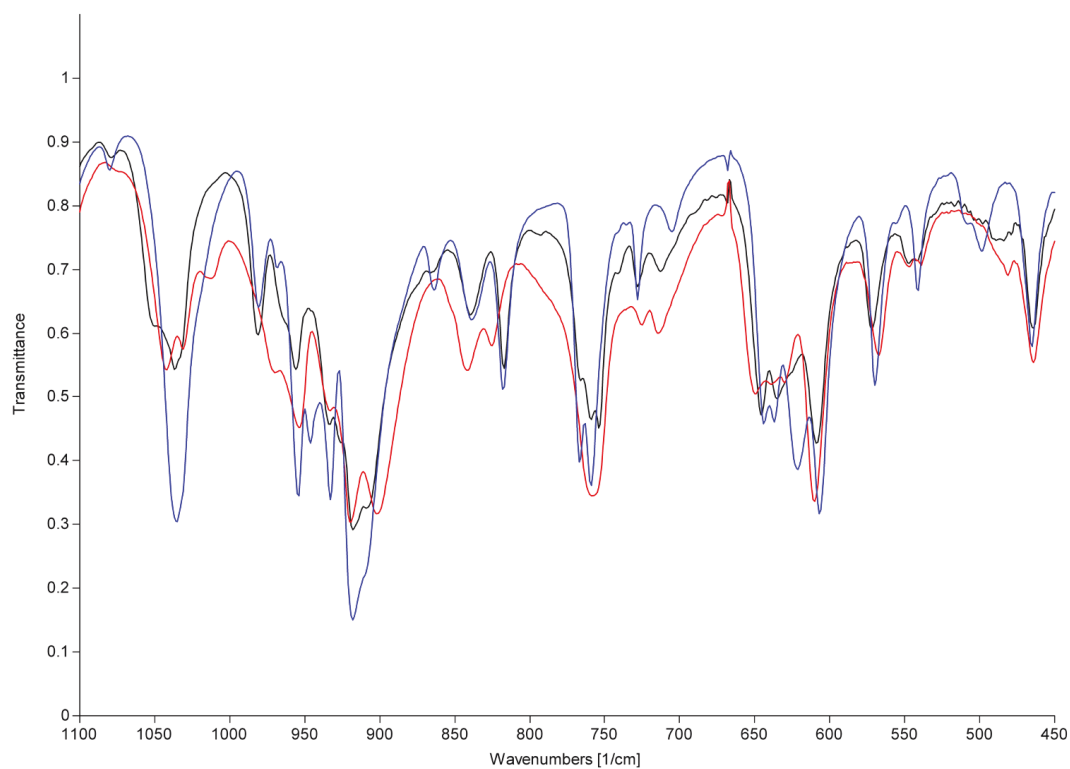
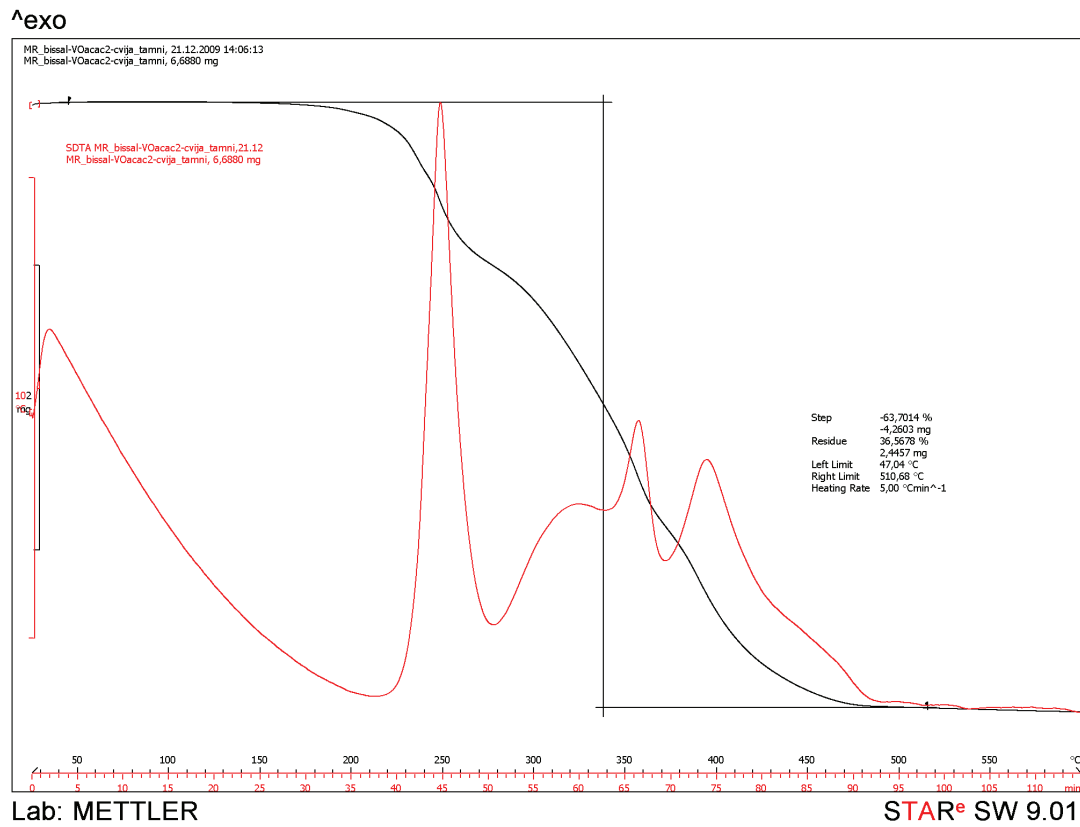
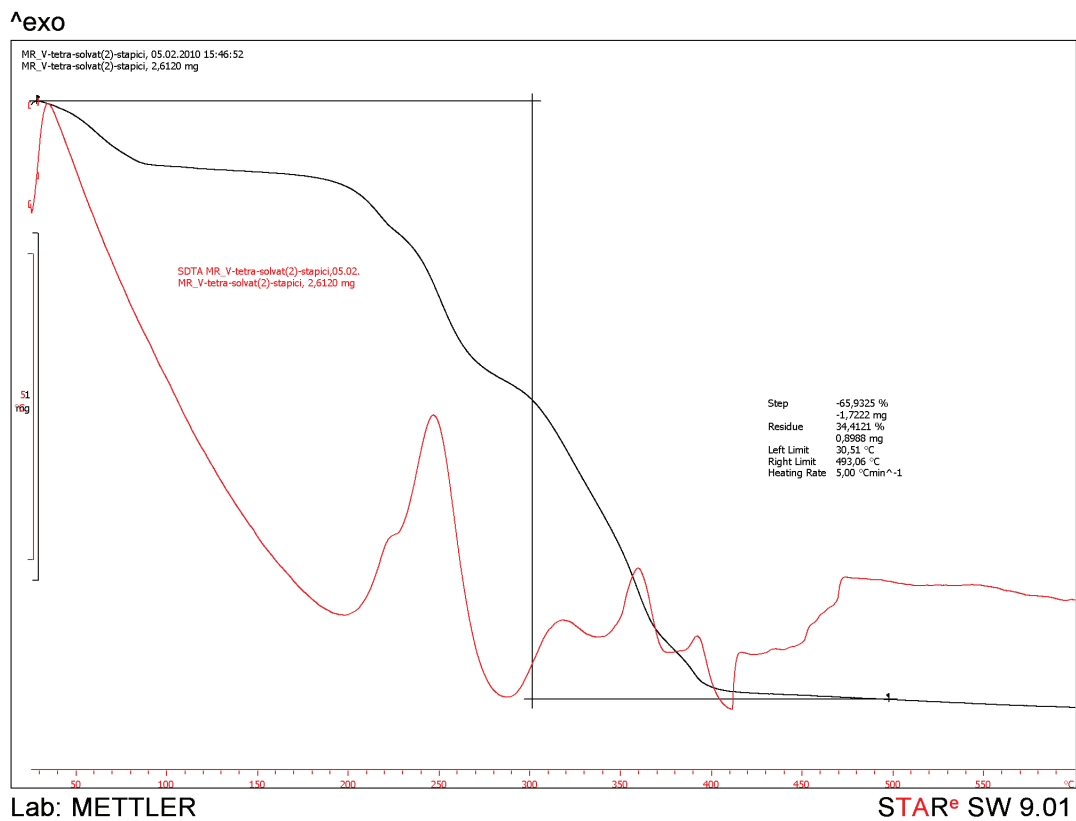


Figure S8. IR spectra and selected maxima for: (a) **1**; (b) **2**; (c) **3**. (d) Comparison of IR spectra of **1**, **2** and **3** in the spectral region below 1100 cm^{-1} .

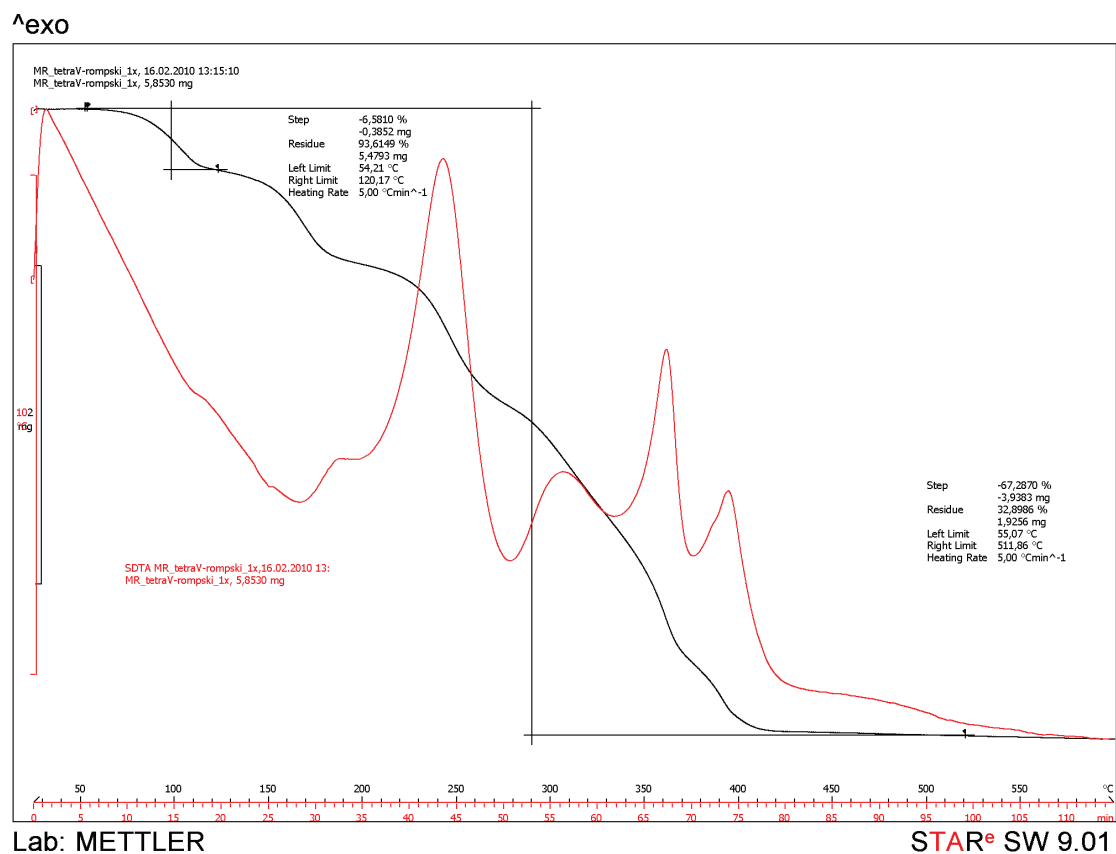
5. Thermal analysis



(a)



(b)



(c)

Figure S9. TGA/DTA curves for the compounds:

(a) $[\text{V}_2\text{O}_3(\text{HL})(\text{OCH}_3)]_n$ (**1**);

(b) $\{[\text{V}_2\text{O}_3(\text{HL})(\text{OCH}_3)] \cdot 2\text{CH}_3\text{OH}\}_n$ (**2**) and

(c) $[\text{V}_2\text{O}_3(\text{HL})(\text{OCH}_3)]_2 \cdot 4\text{CH}_3\text{OH}$ (**3**). For **3**, the weight loss in the first step roughly corresponds to half of the methanol molecules found in the sample. The remaining methanol molecules depart during the second step in which degradation of the sample also begins.

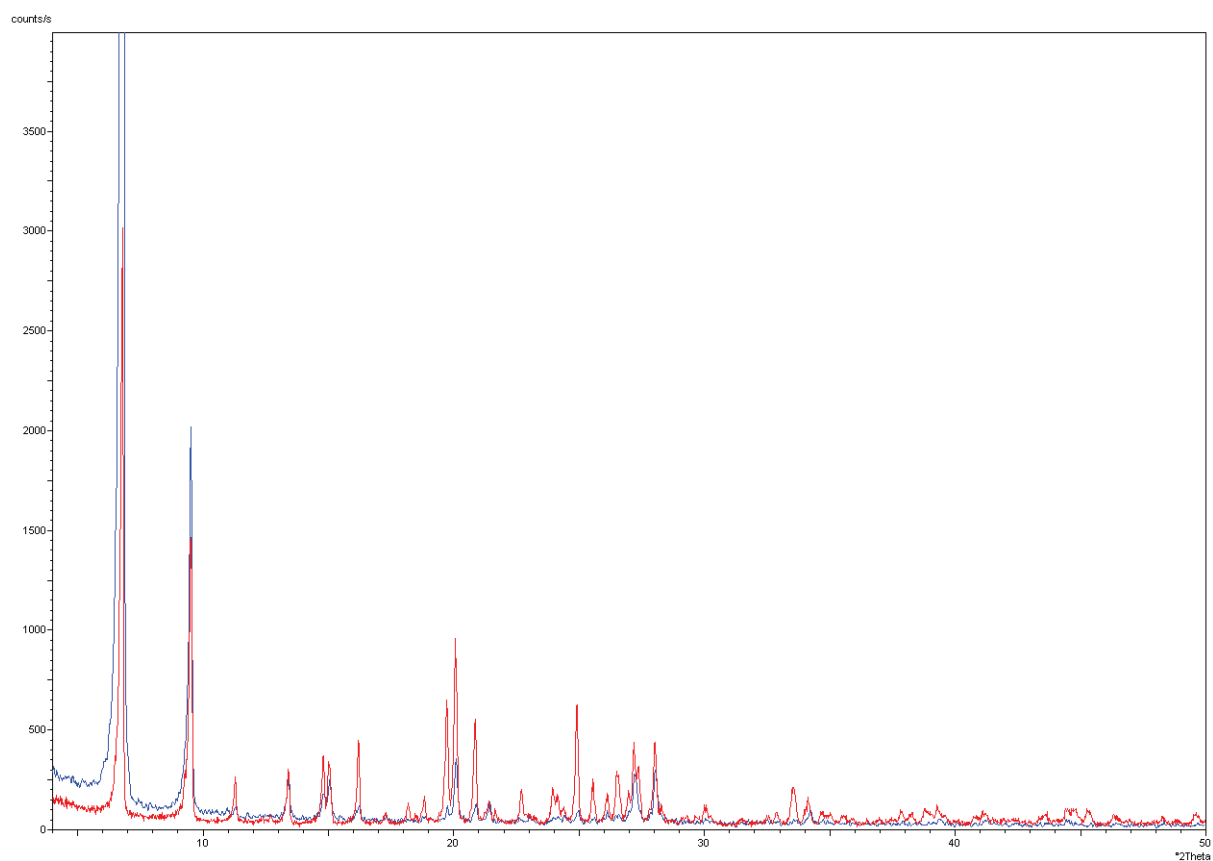


Figure S10. Comparison of diffraction patterns of pure compound $\{[V_2O_3(HL)(OCH_3)]\}_n$ (**1**) (red) and the material obtained after 8h of slurring mixture of compounds **1**, **2** and **3** at methanol boiling point (blue).

6. References

- [1] V. Favre-Nicolin, R. Černý, *J. Appl. Cryst.* **2002**, 35, 734-743.
- [2] Topas, version 4.1 Bruker-AXS, Karlsruhe, Germany